Journal of Alloys and Compounds 503 (2010) 375–379

Contents lists available at ScienceDirect

Journal of Alloys and Compounds

journal homepage: www.elsevier.com/locate/jallcom

Order-sintering of mechanically alloyed FeAl nanostructures

Sh. Ehtemam Haghighi [a], K. Janghorban [a], S. Izadi [b,*]

[a] Department of Materials Science and Engineering, School of Engineering, Shiraz University, Zand Blvd, 7134851154, Shiraz, Iran
[b] Department of Material Science and Engineering, Shahid Bahonar University of Kerman, 76135-133, Kerman, Iran

ARTICLE INFO

Article history:
Received 26 November 2009
Received in revised form 16 March 2010
Accepted 17 March 2010
Available online 23 March 2010

Keywords:
Nanostructured materials
Sintering
X-ray diffraction
Order–disorder effects

ABSTRACT

In this work, FeAl intermetallic compounds were prepared by mechanical alloying and subsequent sintering processes. The powder milled for 80 h was found to be disordered Fe(Al) nanocrystals with 15 nm in size, which was sintered at 900 and 1000 °C for 1, 3 and 5 h. X-ray diffraction studies of the samples revealed a microstructural evolution and ordering during sintering. At both the sintering temperatures, the long-range order parameter first increased due to the promotion of ordered FeAl from the disordered Fe(Al) solid solution and then decreased by increasing the sintering time. This behavior was attributed to an increase in the concentration and clustering of thermal vacancies. It was also found that by increasing the sintering time, the crystallite size and lattice strain decreased, whereas the relative density and hardness increased.

1. Introduction

Mechanical alloying (MA) is a feasible technique to make intermetallics like FeAl. This compound has some attractive properties, especially a considerable corrosion resistance under oxidizing, sulfidizing and carburizing atmospheres. In addition, it has a high electrical resistivity (130–170 μΩ/Cm), which is comparable to many commercial metallic heating elements [1–4]. However, its drawback is its brittleness at medium and low temperatures. It is assumed that its ductility would be enhanced by nano-sized crystals [2].

The FeAl phase diagram shows that it forms at a composition range of 36–50 at.% Al [4]. Previous studies emphasize that FeAl contains a unique thermal vacancy concentration compared to all iron aluminides, estimated to several percent [5]. This is due to the low enthalpy of vacancy formation (ΔH_f) which decreases by increasing the content of Al [5,6] (typically, $\Delta H_f \approx 104$–98 (kJ/mol) for Fe 37–39 at% Al, 93–39 (kJ/mol) for Fe 40–51 at% Al, and 34 (kJ/mol) for Fe–50 at% Al [5]). On the other hand, it was established that the vacancy concentration increases with increasing temperature, cooling rate from high temperatures, and Al content, causing a significant hardening [4]. It is expected that during slow cooling, hot pressing and after quench annealing, the vacancies annihilate at sinks, leading to softening relative to the rapid quench condition where the vacancies stay as single point defects, thereby causing vacancy hardening [5].

It was also shown that vacancies tend to form divacancies and clusters in FeAl [4]. This causes crystals to be divides into sublattices resembling a mosaic substructure that is detectable by X-ray diffraction (XRD) [7]. Since the vacancy concentration and clusters impress almost all behaviors of FeAl, many researches have been conducted to characterize the kinetics, thermodynamics, and structural properties related to both thermal vacancies and quench in vacancies [4,5].

In this work, disordered Fe(Al) nanostructures were prepared by MA. The ordering characteristics were documented by XRD and the effect of vacancy concentration on the crystallite size, lattice strain and order parameter was explored.

2. Experimental methods

A 50 at.% mixture of Fe (99% pure) and Al (99.9% pure) powders was milled in a planetary ball mill at a rotational speed of 300 rpm for 80 h with the ball-to-powder weight ratio of 50:1. To minimize oxidation, milling was conducted under argon and powder sampling was performed 1 h after the milling apparatus was turned off. During MA, some contamination is imminent; however, it was minimized by a special hardened stainless steel mill used in this work. Since only the powder milled for 80 h was considered, the amount of contamination of the milled powder was the same but not detected by XRD. The microstructure of the as-milled powder was investigated by XRD (Philips Analytical PC-APD diffractometer by Cu kα radiation ($\lambda = 0.1542$ nm)). The 80 h MA powder was cold-pressed under 1200 MPa to disks of 10 mm in diameter and 2 mm in thickness. The disks were first encapsulated in sealed quartz tubes evacuated to 10^{-3} torr and then sintered at 900 and 1000 °C for 1, 3 and 5 h. The heating rate was 15 °C/min and the sintered samples were quenched to room temperature in air.

The XRD method was utilized to detect any phase change during sintering. An angular step size of 0.05° and step time of 1 s/step were used. The XRD data of the instrument were smoothened by the Fityk software to obtain the pure broadening of diffraction lines which was then used for the Williamson–Hall calculations. The crystallite size (D) and lattice strain (ε) of the sintered samples at the different test

* Corresponding author. Tel.: +98 917 138 3812; fax: +98 711 230 7293.
E-mail address: saideh_izadi177@yahoo.com (S. Izadi).

0925-8388/$ – see front matter © 2010 Published by Elsevier B.V.
doi:10.1016/j.jallcom.2010.03.150

conditions were calculated by applying the Williamson–Hall formula as:

$$B\cos\theta = \frac{k\lambda}{D} + 2\varepsilon\sin\theta \quad (1)$$

where B is the full-width at half-maximum (FWHM) of a diffraction peak, k is a constant, λ is the X-ray wavelength and θ is the Bragg angle. According to Eq. (1), $\sin\theta$ vs. $B\cos\theta$ was plotted using three peaks of (1 1 0), (2 1 1) and (2 2 0). The crystallite size and lattice strain were then calculated from the intercept and slope of this line, respectively [8].

The long-range order parameter, S, is defined as [9]:

$$S^2 = \frac{I_{S(dis)}/I_{F(dis)}}{I_{S(ord)}/I_{F(ord)}} \quad (2)$$

where $(I_S/I_F)_{dis}$ and $(I_S/I_F)_{ord}$ are the ratio of the integrated intensities (peak area) of the superlattice reflection to the fundamental line for the disordered (dis) and reference (ord) powders, respectively [9]. In this work, the intensity of the (1 0 0) and (2 0 0) diffraction lines was chosen to represent the superlattice and fundamental peaks for the S calculations.

The density of the samples before and after sintering was measured by the Archimedes water immersion method. The pore configuration was observed by scanning electron microscopy (SEM, JEOL-JSM 5310). The microhardness of their pore-free zones was measured using 0.25 N load at eight different spots for better averaging. The indented surface was finally observed by an optical microscope.

3. Results and discussion

The XRD results of the initial powder mixture (Fe–50 at.% Al), the 80 h milled product and the samples sintered at 900 and 1000 °C for the durations of 1, 3 and 5 h are shown in Fig. 1. Fig. 1a indicates that 80 h of milling results in the development of a single phase, a disordered solid solution (Fe(Al)). This transformation has been also reported by other researchers [10–19]. The lattice strain and crystallite size of the milled powder are 3.1% and 15 nm, respectively. It is noted that the crystallite size of Fe–50 at.% Al powder milled for 50 h in a SPEX is reported to approach 7 nm [17], due to the higher energy of SPEX. On the other hand, the sintering of the powder promotes ordering and the appearance of FeAl intermetallic, as recorded by the superlattice reflections in their XRD patterns (Fig. 1b and c). These patterns also show less peak broadening compared to the milled sample, which indicates a reduction in lattice strain and some grain growth during sintering. It has been pointed out that sintering at 700 °C for 30 min under an uniaxial pressure of 2 GPa increases the crystallite size of mechanically alloyed Fe–50 at.% Al powder from 7 to only 21 nm [17], due to the low sintering time and temperature and the application of the high pressure restricting migration of grain boundaries. Several authors have consolidated Fe–Al under high pressures obtaining nanocrystalline grain size [1,17,20]. The lattice strain and crystallite size for the sintered samples are depicted in Fig. 2, determined by the Williamson–Hall analyses. According to these figures, in both sintering temperatures a reduction in the lattice strain and crystallite size by increasing the sintering time occurs. Whereas it is expected to have grain growth during sintering at high temperatures like 900 and 1000 °C rather than the shrinkage of grain size.

The source of this abnormal trend in the grain size behavior is the high concentration of equilibrium vacancies in FeAl at temperatures above 700 °C, which is the highest content among all aluminides due to the low enthalpy of the vacancy formation in FeAl ($\Delta H_f \approx 63$ kJ/mol) [4]. It is inferred that these vacancies individually or in clusters generate subgrains which were detected by the XRD analysis. Indeed, grain growth has occurred at the high sintering temperatures; however, the vacancy clusters divide each grain to finer subgrains and produce a mosaic substructure which was revealed by the XRD analysis [7]. These high concentrated vacancies also are very effective in reducing the lattice strain by the annihilation of site defects produced during MA. The vacancy concentration increases in FeAl by sintering time, although reaches to an equilibrium concentration at short time ~10 min [5]. Afterwards, the vacancy rearrangement occurs, dividing each grain to the finer subgrains. This explains the reduction of the lattice strain

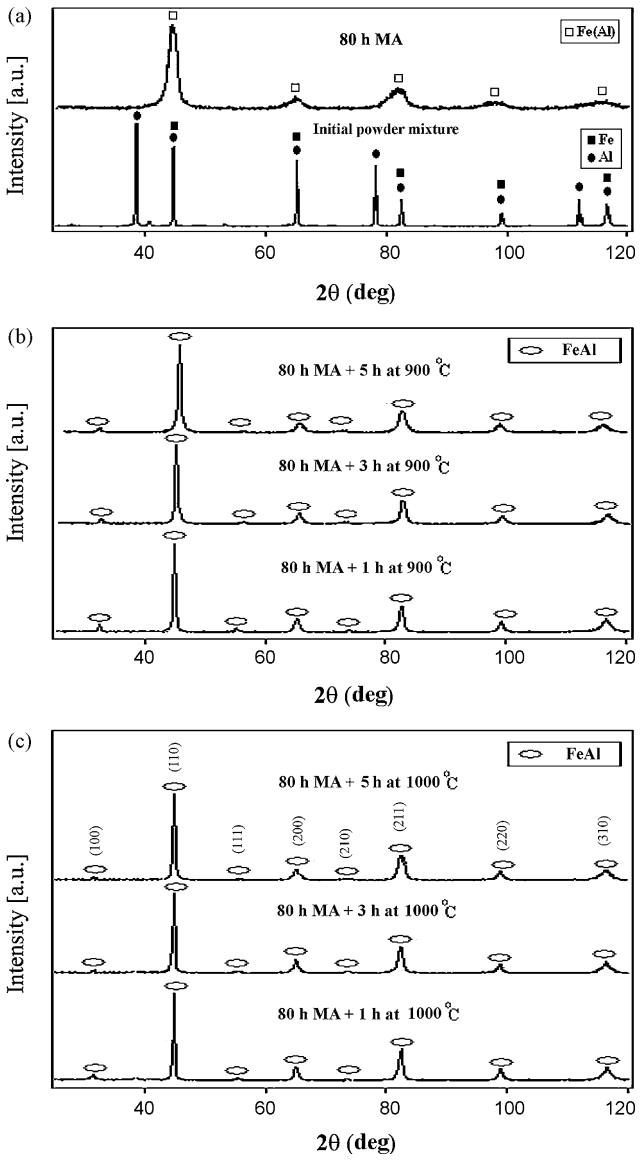

Fig. 1. XRD patterns of the initial powder mixture and the powder milled for 80 h (a); the milled powder sintered at 900 °C for the various times (b); and the powder sintered at 1000 °C for the various times (c). Comparing the reflections of the as-milled and sintered powders suggests that the (1 1 0), (2 0 0), (2 1 1), (2 2 0), and (3 1 0) reflections are the fundamental reflections and the other ones are superlattice reflections.

and crystallite size as well as the long-range order parameter by the passage of sintering time at 900 and 1000 °C (Fig. 3). As showed in Figs. 2 and 3, the differences between the crystallite size, strain, and order parameter are so insignificant that it is difficult to recognize visually the differences in the peak intensity and broadening in the XRD patterns of Fig. 1. By increasing the sintering time at each sintering temperature, the decrease in the crystallite size and strain dictates opposite trends in the evolution of broadening, making the variation of broadening insignificant visually. However, it seems that the contribution of the size evolution to broadening prevails over that of the strain evolution. On the other hand, the broadening in the samples sintered at 1000 °C is smaller than that for the samples sintered at 900 °C, as expected form the crystallite size and strain evolutions demonstrated in Fig. 2. In addition, the decrease in the intensity of the superlattice peaks over that of the fundamental reflections verifies the results of Fig. 3.

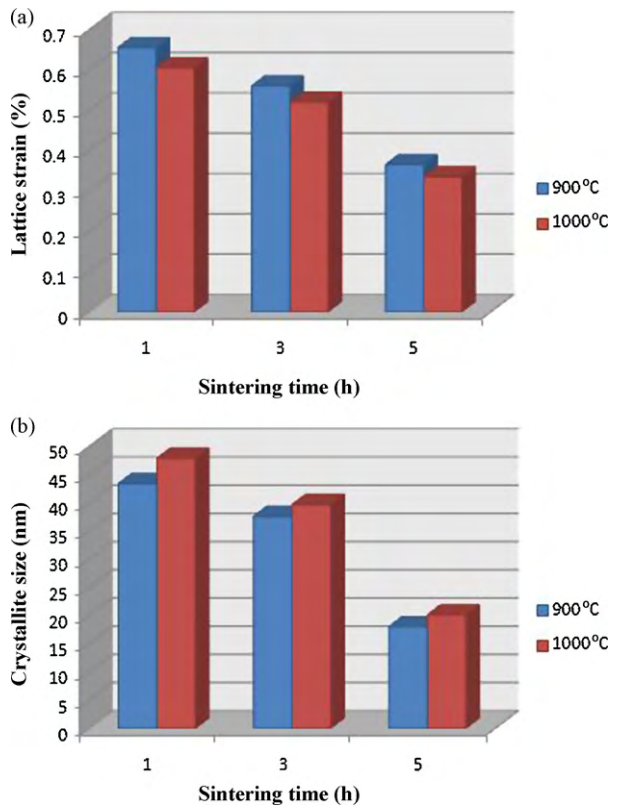

Fig. 2. Lattice strain (a) and crystallite size (b) as a function of sintering time at 900 and 1000 °C.

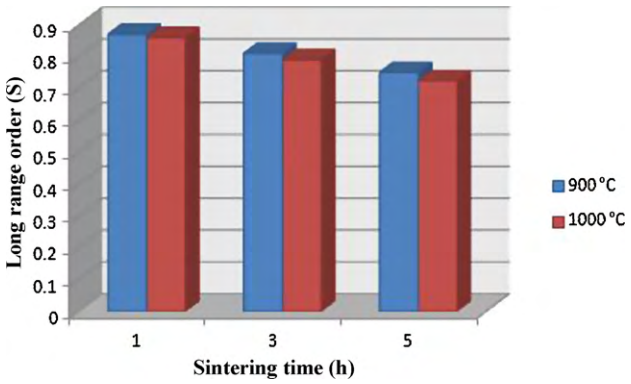

Fig. 3. Long-range order parameter as a function of sintering time.

Sintering for 1 h enhances ordering and promotes the transformation of the disordered Fe(Al) to ordered FeAl with a B2 structure; nonetheless, the longer sintering durations reverse the process and decrease the order parameter from 0.86 (1 h) to 0.72 (5 h) at 1000 °C. This effect is explained by the role of the high vacancy concentration. During the early stages of sintering, vacancies annihilate site defects and accordingly ordering of FeAl is promoted. At longer sintering durations, more vacancies are generated and mostly combine to form vacancy clusters which destroyed the ordered structure. In other words, the individual vacancies accelerate diffusion and ordering; in contrast, clustering makes them less mobile and destroys the ordered lattice to extents detected by the XRD analyses.

Another microstructural evolution during sintering was densification and the decrease of microporosities. Fig. 4 demonstrates the relative density of the sintered specimens. The higher sintering temperatures and times give the higher densities. This implies

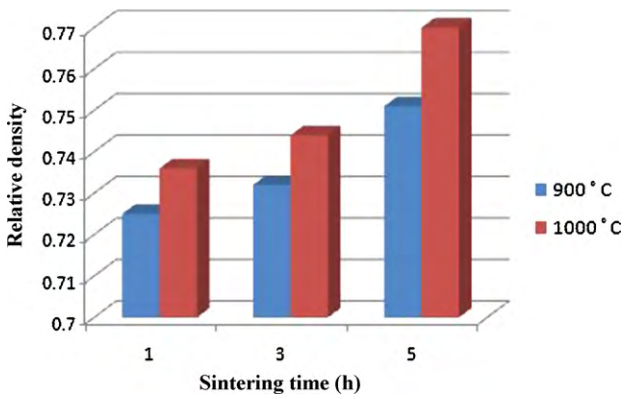

Fig. 4. Relative density as a function of sintering time at 900 and 1000 °C.

that the increase in the number of vacancies and clusters at the higher sintering temperature and time was not comparable to the shrinkage of microporosities; and eventually the net effect was the densification.

The SEM micrographs of the surface of the samples sintered at 900 and 1000 °C for 1 and 5 h are shown in Fig. 5. Note that the black spots are open pores. These figures show a decreasing trend in the number and size of pores at the higher sintering temperatures and durations, which is due to higher diffusion rate and/or more time for densification.

Less porosity results in a higher hardness, as revealed by the microhardness measurements shown in Fig. 6. The increased hardness at the higher sintering temperatures is due to a combined effect of lower porosity (at the microscopic level) and vacancy hardening (at the atomic level). As mentioned earlier, FeAl contains a high concentration of thermal vacancies, causing structure hardening through the relationship $H_V \alpha C_V^{1/2}$, where H_v is the hardness and C_v is the vacancy concentration [4,5]. The vacancy hardening mechanism is the well-known pinning and blocking of mobile dislocations to suppress plastic deformation [5], which induces brittleness. However, the studied samples present the lower hardness values than the microhardness of nanocrystalline FeAl intermetallic prepared by mechanical alloying and sintering reported in Refs. [14,17,20]. It is attributed to the contributions of the retained pores and larger nanograins developed in this work in comparison with Refs. [14,17,20].

Fig. 7 depicts elongated cracks initiating from the indented regions during the microhardness tests. This is an indication of the brittleness of the sintered sample, which was rapidly cooled to room temperature. The comparison of the present work with the hot-pressed FeAl at 400, 500, 600, 700, 800 and 900 °C [20] suggests major differences. In the hot-pressed samples, the crystallite size and long-range order parameter increase with temperature, whereas these parameters decrease under the sintering and rapid quench conditions of this work. These discrepancies can be explained in terms of the behavior of thermal vacancies under the two different test conditions. In the sintering conditions of the present work, the more exposure durations at the high temperatures is available in comparison to hot pressing which limits the time considerably [21]. This prolonged time leads to more vacancy generation and combination to form the clusters. On the other hand, applying high pressures in hot pressing can hinder the cluster formation, as well as limiting the high temperature exposure time. This is due to the fact that the vacancy migration, leading to the formation of the clusters, is a diffusion process and the high pressures can decrease the diffusion coefficient. Thus, the less mobile clusters formed in this work are trapped and cannot migrate to sinks upon the subsequent rapid quenching [22]. Nonetheless, during

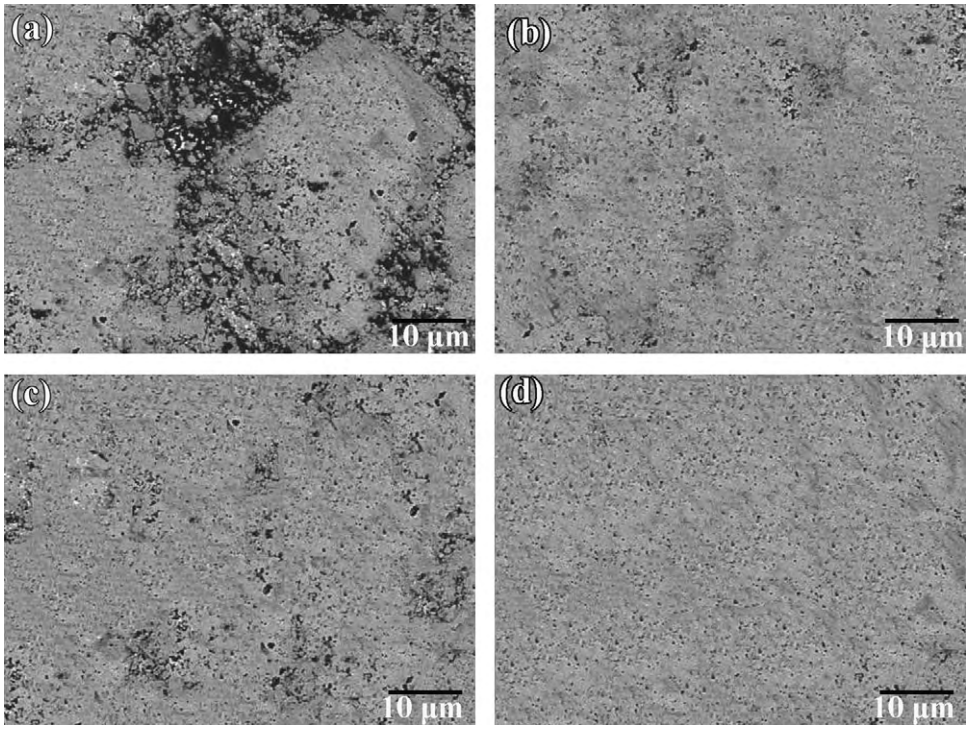

Fig. 5. SEM micrographs of the samples sintered at 900 °C for 1 h (a), 5 h (b), at 1000 °C for 1 h (a) and 5 h (b).

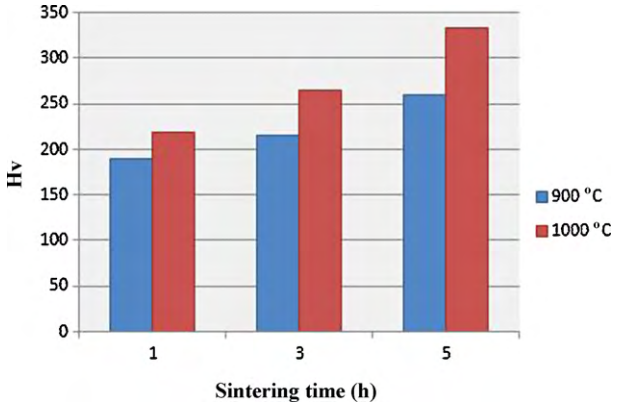

Fig. 6. Vickers microhardness as a function of sintering time.

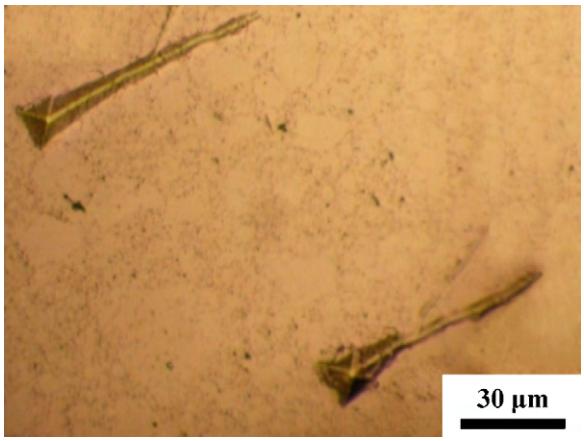

Fig. 7. Optical image of the elongated cracks originating from the indented regions during the indentation.

hot pressing, the vacancy concentration decreases as the vacancies annihilate at sinks to the extent that their presence does not hinder ordering; consequently, the ordered structure was preserved. For the same reason, the grains are not divided to subgrains by the vacancy clusters and the grain size increases with the temperature of the hot pressing process.

4. Conclusions

1. The sintering of the mechanically alloyed powders resulted in an grain growth, the reduction of the lattice strain and the transformation of the disordered Fe(Al) to the ordered FeAl intermetallic.
2. At both the sintering temperatures of 900 and 1000 °C, the high concentrations of the thermal vacancies and their clustering led to the subgrain formation and accordingly a decrease in ordering at the longer sintering durations.
3. The density increased due to the pore elimination at the high sintering temperatures and durations.
4. The hardness of the sintered samples increased due to the pore elimination and vacancy hardening due to the presence of the quenched vacancies at room temperature. Both the effects caused the brittleness of the samples.

References

[1] M. Krasnowski, T.J. Kulik, Intermetallics 15 (2007) 201–205.
[2] H.W. Shi, K. Guo, J. Alloys Compd. 455 (2008) 207–209.
[3] M. Krasnowski, A. Grabias, T. Kulik, J. Alloys Compd. 424 (2006) 119–127.
[4] J.L. Jordan, S.C. Deevi, Intermetallics 11 (2003) 507–528.
[5] O. George, D.G. Morris, M.A. Morris, Mater. Sci. Eng. A 258 (1998) 99–107.
[6] J.H. Schneibel, Mater. Sci. Eng. A258 (1998) 181–186.
[7] B.D. Culity, Elements of X-Ray Diffraction, Addison-Wesley Publishing Company, Inc., New York, 1978.
[8] W.H. Hall, G.K. Williamson, Acta Metall. 1 (1953) 23–31.
[9] I. Baker, Q. Zeng, Intermetallics 14 (2006) 396–405.
[10] F. Cardellini, V. Contini, G. Mazzone, J. Mater. Sci. 31 (1996) 4175–4180.
[11] F. Cardellini, V. Contini, R. Gupta, G. Mazzone, A. Montone, A. Perin, G. Principi, J. Mater. Sci. 33 (1998) 2119–2127.

[12] E. Bonetti, G. Scipione, G. Valdré, G. Cocco, R. Frattini, P.P. Macrí, J. Appl. Phys. 74 (3) (1993) 2053–2057.
[13] E. Enzo, R. Frattini, R. Gupta, P.P. Macrí, G. Principi, l. Schiffini, G. Scipione, J. Acta Mater. 44 (8) (1996) 3105–3113.
[14] F. Charlot, E. Gaffet, B. Zeghmati, F. Bernard, J.C. Niepce, Mater. Sci. Eng. A262 (1999) 279–288.
[15] L. D'Angelo, G. González, J. Ochoa, J. Metastable Nanocrystal. Amorphous Mater. 20–21 (2004) 231–236.
[16] D.A. Eelman, J.R. Dahn, G.R. Mackay, R.A. Dunlap, J. Alloys Compd. 266 (1998) 234–240.
[17] L. D'Angelo, L. D'Onofrio, G. Gonzalez, J. Alloys Compd. 483 (2009) 154–158.
[18] S. Izadi, K. Janghorban, G.H. Akbari, M. Ghafari, E. Salahinejad, J. Alloys Compd. 493 (2010) 645–648.
[19] Sh. Ehtemam Haghighi, K. Janghorban, S. Izadi, J. Alloys Compd. (2010), doi:10.1016/j.jallcom.2010.01.145.
[20] M.A. Morris-Munoz, A. Dodge, D.G. Morris, NanoStruct. Mater. 11 (1999) 873–885.
[21] M. Krasnowski, T. Kulik, Intermetallics 15 (2007) 1377–1383.
[22] M.A. Morris, O. George, D.G. Morris, Mater. Sci. Eng. A 258 (1998) 99–107.